

Tracing the Outer Structure of the Sagittarius Dwarf Galaxy: Detections at Angular Distances Between 10 and 34 Degrees *

Mario Mateo¹

e-mail: mateo@astro.lsa.umich.edu

Edward W. Olszewski²

e-mail: eolszewski@as.arizona.edu

Heather L. Morrison³

e-mail: heather@vegemite.cwru.edu

Received _____; accepted _____

*Based on observations obtained with the Blanco Telescope at CTIO, which is operated by the National Optical Astronomy Observatory, under contract to AURA.

¹Department of Astronomy, University of Michigan, 821 Dennison Bldg., Ann Arbor, MI 48109-1090

²Steward Observatory, 933 N. Cherry, University of Arizona, Tucson, AZ 85721-0065

³Cottrell Scholar of Research Corporation, and NSF Career Fellow; Department of Astronomy and Department of Physics, Case Western Reserve University, Cleveland OH 44106

ABSTRACT

We have obtained deep photometric data in 24 fields along the southeast extension of the major axis of the Sagittarius dwarf spheroidal (Sgr dSph) galaxy, and in four fields along the northwest extension. Using star counts at the expected position of the Sgr upper main-sequence within the resulting color-magnitude diagrams (CMDs), we unambiguously detect Sgr stars in the southeast over the range $10\text{--}34^\circ$ from the galaxy’s center. If Sgr is symmetric, this implies a true major-axis diameter of at least 68° , or nearly 30 kpc if all portions of Sgr are equally distant from the Sun. Star counts parallel to the galaxy’s minor-axis reveal that Sgr remains quite broad far from its center. This suggests that the outer portions of Sgr resemble a stream rather than an extension of the ellipsoidal inner regions of the galaxy. The inferred V-band surface brightness (SB) profile ranges from $27.3\text{--}30.5$ mag arcsec $^{-2}$ over this radial range and exhibits a change in slope $\sim 20^\circ$ from the center of Sgr. The scale length of the outer SB profile is 17.2° , compared to 4.7° in the central region of Sgr. We speculate that this break in the SB profile represents a transition from the main body of Sgr to a more extended ‘Sgr stream’. By integrating the SB profile we estimate that the absolute visual magnitude of Sgr lies in the range -13.4 to -14.6 , depending on the assumed structure of Sgr; an upper limit to the luminosity of Sgr is therefore $L \sim 5.8 \times 10^7 L_\odot$. This result lowers the M/L_V ratio inferred for Sgr by Ibata et al. (1997) down to ~ 10 , consistent with values observed in the most luminous dSph companions of the Milky Way.

Subject headings: Galaxy: halo — Galaxy: structure — galaxies: individual (Sgr dSph) — galaxies: interactions — galaxies: Local Group

1. Introduction

Since its discovery in 1994 (Ibata et al.), the known extent of the Sagittarius dwarf galaxy (Sgr) has grown steadily. The first map revealed a galaxy with a possibly clumpy structure subtending a region about $8^\circ \times 5^\circ$ in size, and oriented roughly perpendicular to the Galactic plane. Subsequently, a series of papers reported a far larger projected size of at least $20^\circ \times 8^\circ$ for Sgr (Mateo et al. 1996; Alard 1996; Fahlman et al. 1996; Ibata et al. 1997; Alcock et al. 1997) based on observations of various stellar tracers. Recently, Siegel et al. (1997) reported a possible detection of Sgr far beyond this $20^\circ \times 8^\circ$ boundary.

Because Sgr is located only 16 kpc from the center of the Milky Way (Ibata et al. 1994; Mateo et al. 1995), there is universal agreement that it is experiencing a strong tidal encounter. Generic simulations of dwarf-satellite destruction, as well as models specific to Sgr (Allen and Richstone 1988; Moore and Davis 1994; Piatek and Pryor 1995; Oh et al. 1995; Johnston et al., 1995; Velazquez and White 1995; Ibata et al. 1997; Zhao 1998) reveal that a strong tidal encounter will draw leading and trailing tidal streams out from the main body of Sgr during its closest encounters with the Milky Way. These streams should extend close to the projected major axis of the galaxy as stars migrate along orbital paths close to that of the disintegrating system. Evidence already exists for extra-tidal stars in some halo systems (globulars, Grillmair et al. 1995; dSph's, Kuhn et al. 1996, see discussion in Olszewski 1998). In this *Letter* we report the systematic search for and discovery of a distinct tidal stream of stars associated with Sgr but extending nearly three times further from the center of Sgr than previously published.

2. Observations and Reductions

We obtained data on two photometric nights (July 1/2 and 2/3, 1998) with the BTC CCD array at the prime focus of the Blanco 4m telescope at CTIO. Because of charge-transfer problems with Chip 1 of the BTC, we did not use results from this CCD in our analysis; thus, each CMD represents counts from 0.19 deg^2 on the sky. We generally obtained single exposures in V and I (typically 10-12 min duration each) in every field. An automatic pipeline procedure (Unix and IRAF daemons) was developed to process the frames with no intervention and in near real time. Data were archived, overscan, zero and flatfield corrected, reduced using the DoPhot photometry program, and combined to make instrumental CMDs. Results for three Sgr fields and their control fields are shown in Figure 2. The CCDs were individually calibrated using numerous observations of Landolt (1992) standards. The photometric transformations for I and $(V-I)$ showed a scatter of less than 1.5% on both nights.

Our goal was to identify main-sequence stars in Sgr along the extension of its major axis, the position angle (PA) of which we originally took to be 109.2° (we present a better estimate of this angle below). The center of Sgr was assumed to coincide with the globular cluster M 54. The locations of the 17 major-axis fields to the southeast are shown in Figure 1 and their equatorial and Galactic coordinates are listed in Table 1. We also observed seven control fields located symmetrically opposite of the $l = 0^\circ$ meridian from the corresponding target fields (see Figure 1 and Table 1), and four fields perpendicular to the major axis of Sgr and passing through Field 3 (denoted as Fields 3-S n and 3-N n for the fields south and north of Field 3, respectively, in Table 1). The angular separation of each field from the center of Sgr is denoted as R in Table 1.

3. Analysis and Results

The Sgr main sequence turnoff occurs at $I_0 \sim 20$ mag and $(V-I) \sim 0.6$ (Mateo et al. 1996; Fahlman et al. 1996; Figure 2). By good fortune, this corresponds to a gap in the density of contaminating foreground stars from the thin disk (located at $I_0 \lesssim 20$ in this color range) and background galaxies that populate the prominent ‘blob’ in Figure 2 fainter than $I_0 \sim 22.5$ at this color. To improve contrast, we counted stars only within the box shown in the first panel of Figure 2. Subtracting the counts from a control field statistically removes non-Sgr stars in the box. The reddening at every field center was taken from the extinction maps of Schlegel et al. (1998; see Table 1); we shifted the selection box accordingly before counting stars. At the lowest Galactic latitudes the 3-chip BTC area contains about 10^4 stars; typical separations of all detected objects are therefore 10 times the seeing diameter. From past experience (e.g. Hurley-Keller et al. 1998), we conclude that completeness corrections are negligible in all of our fields.

The upper panel of Figure 3 shows the main-sequence counts along the Sgr major-axis and for the control fields. The effects of systematic changes in the adopted $(V-I)$ reddening by ± 0.03 mag are also illustrated. Even in the outermost Sgr point – Field 17 located at $R = 34^\circ$ – there is a clear excess of stars relative to the controls. Note that the *raw* Sgr counts exhibit a clear change in the slope of the density profile at $R \sim 20^\circ$.

To correct for contamination by Galactic stars, we fit a straight line to the control-field counts (Fig 3), subtracting the fitted counts from the raw Sgr counts. The net counts are plotted as a function of R in the lower panel of Figure 3. Mateo et al. (1996) estimated that the V-band surface brightness (SB) at the innermost field in this study ($R \sim 10^\circ$) is $\Sigma_V = 27.3$. Normalizing to this value, we can express the star counts in SB units as shown in the lower panel of Figure 3. We assume that there are no spatial variations in the stellar population within Sgr, a point supported by star counts in other regions of our CMDs. The

SB of the outermost Sgr fields, where we detect a $4\text{-}6\sigma$ excess over the control field counts, is $\Sigma_V \sim 30.5 \text{ mag arcsec}^{-2}$.

Since a tidal stream should consist of leading and trailing components, we also observed fields at 30° and 40° along the northwest major axis extension. However, the large and rapidly variable reddening at $(l,b) = (3,16)$ and $(2,26)$ caused this first attempt to fail. Siegel et al. (1997) also failed to find Sgr more than 40° towards the northwest at $(l,b)=(353,41)$.

4. Discussion

Given the clear break in the star-count profile in Figure 3, we have fit the net counts with two exponential profiles. The best-fit composite profile is plotted in Figure 3 and can be decomposed as:

$$\Sigma_{V,inner} = 25.25 + 0.23R,$$

$$\Sigma_{V,outer} = 28.55 + 0.063R,$$

where Σ is in mag arcsec^{-2} , and R in degrees. Due to time lost to poor weather, our data perpendicular to the major axis are limited so far to the one cross-cut centered on Field 3 (see Figure 1). Taking z to be the angular separation from the major axis along this cross-cut (in degrees), we find that a Gaussian profile adequately fits the data:

$$\Sigma_{cc,3} = 27.84 + 0.071z^2.$$

The constant reflects the fact that the centroid of $\Sigma(z)$ relation is about 1° north of Field 3. Either we did not precisely follow the ‘true’ major axis of Sgr, or else the galaxy’s projected stellar density distribution does not follow a great circle. In the former case, we conclude that the true major-axis PA of Sgr is $104.8^\circ \pm 1.2^\circ$. To test for curvature, more cross-cuts are required. The Siegel et al. (1997) field is $\sim 2^\circ$ north of our Field 12. Their detection of Sgr is consistent with the smaller PA, and with the broad width of Sgr at this location.

Despite Field 17 being $\sim 2.5^\circ$ away from the ideal position, it still unambiguously shows Sgr, 7.5° further from the center of Sgr than the Siegel et al. field.

If we extrapolate the composite exponential profile in Figure 3 to the center of Sgr, the inferred central SB is $\Sigma_{0,V} = 25.2 \pm 0.3 \text{ mag arcsec}^{-2}$, close to the value estimated by Mateo et al. (1995). Ibata et al. (1997) found that the radial profile of Sgr is well fit by a King-profile with a core radius of $\gtrsim 1.3^\circ$. Since exponential and King-model profiles fit low-concentration systems equally well (e.g., Eskridge 1988), these results are not incompatible. We also note that the smooth exponential profiles do not seem to perfectly match the observations on $3\text{--}5^\circ$ scales (Figure 3; note the Poisson error bars). This implies that the SB distribution of Sgr may be clumpy in its outer regions (Mateo et al. 1996); further data are needed to confirm this.

We consider two possible cases to estimate the total luminosity of Sgr. First, the inner exponential is taken to represent the ‘main body’ of Sgr with a 3:1 axis ratio (Ibata et al. 1997), while the outer profile represents a tidal stream of constant width as defined by the Gaussian $\Sigma(z)$ relation above. By integrating these profiles, we derive an integrated apparent magnitude of $V_{tot,1} = 3.6$ for Sgr. If the distance modulus over the entire extent of the galaxy is assumed constant at $(m - M)_0 = 17.0$ (Ibata et al. 1994; Mateo et al. 1995; Ibata et al. 1997; though see Alcock et al. 1997), then $M_{V,tot,1} = -13.4 \pm 0.3$. A second approach is to assume that the width of Sgr is constant at all values of R , again obeying the $\Sigma(z)$ relation derived above. For this case, $V_{tot,2} = 2.7 \pm 0.3$, and $M_{V,tot,2} = -14.3$. Previous estimates of the integrated absolute magnitude of Sgr range from -13 to -13.5 (Ibata et al. 1994; Mateo et al. 1996; Ibata et al. 1997). If we correct for the slight offset of our major axis from the ‘true’ major axis (which slightly increases the radial scale lengths), we can raise the integrated luminosity of Sgr to at most $M_{V,tot,1} \geq -13.8$ and $M_{V,tot,2} \geq -14.6$. Unless an additional outer component of Sgr remains to be discovered, it

seems very unlikely that the integrated V-band absolute magnitude of Sgr is brighter than -14.6 , corresponding to $L_{Sgr,tot} \leq 5.8 \times 10^7 L_{\odot}$.

An important possible consequence of this result is that the inferred V-band M/L ratio of Sgr could drop from ~ 50 (Ibata et al. 1997) to a value as low as ~ 10 with our larger estimate of the total luminosity of Sgr. This lower mass-to-light ratio brings Sgr into better consistency with the M/L ratios observed in other dSph satellites of the Milky Way and M31 (Bellazzini et al. 1996; Mateo 1998).

Perhaps the most interesting feature of the radial profile of Sgr is the kink at $R \sim 20^{\circ}$. Does this represent the transition from a dynamically distinct portion of the Sgr dwarf and a tidal stream – the ‘Sgr stream’ – pulled out of the galaxy? Or are we seeing the current (inner) tidal stream in the process of joining an older, more extended stream from a previous tidal encounter (Zhao 1998)? One key to addressing these questions will be to define the orbital path of Sgr by determining distances along the stream, as attempted by Alcock et al. (1997), and to better define the projected distribution of Sgr stars on the sky. The only well-populated features in the Sgr CMD in these outer fields are the main sequence and sub-giant branch, neither of which are well suited for precise distance determinations. Nevertheless, we have unambiguously detected Sgr at an angular distance that implies overall dimensions of at least $68^{\circ} \times 8\text{-}10^{\circ}$, or about 30×4 kpc. Since the projected scale length of the outer parts of Sgr is 17.2° , we should be able to use the techniques described in this paper to trace the galaxy $20\text{-}30^{\circ}$ further out than we have mapped it so far. Wide-field time series observations along the stream may reveal RR Lyr variables or dwarf Cepheids that can be used to determine precise distances along the outer extension of the Sgr dwarf.

5. Acknowledgements

The authors have been supported by NSF grants AST 9619490 and AST 9619524. We thank Mauricio Fernandez for his help at the 4m telescope, and the entire CTIO staff for their good cheer during abysmal – at times, apocalyptic – weather over the past three observing seasons. We thank Gary Bernstein, Denise Hurley-Keller, Craig Kulesa and Tim Pickering for help in producing Figure 1.

REFERENCES

- Alard, C. 1996, *ApJ*, 458, L17.
- Alcock, C., et al. 1997, *ApJ*, 474, 217.
- Bellazzini, M., Fusi Pecci, F., & Ferraro, F. R. 1996, *MNRAS*, 278, 947.
- Eskridge, P. B. 1988, *AJ*, 96, 1352.
- Fahlman, G. G., Mandushev, G., Richer, H. B., Thompson, I. B., & Sivaramakrishnan, A. 1996, *ApJ*, 459, L65.
- Grillmair, C. J., Freeman, K. C., Irwin, M., & Quinn, P. 1995, *AJ*, 109, 2553.
- Hurley-Keller, D., Mateo, M., & Nemeč, J. 1998, *AJ*, 115, 1840.
- Ibata, R. A., Gilmore, G., Irwin, M. J. 1994, *Nature*, 370, 194.
- Ibata, R. A., Wyse, R. F. G., Gilmore, G., Irwin, M. J., & Suntzeff, N. B. 1997, *AJ*, 113, 634.
- Johnston, K. V., Spergel, D. N., & Hernquist, L. 1995, *ApJ*, 451, 598.
- Kuhn, J. R., Smith, H. A., & Hawley, S. L. 1996, *ApJ*, 469, L93.
- Landolt, A. U. 1992, *AJ*, 104, 340.
- Mateo, M. 1998, *ARAA*, 36, 435.
- Mateo, M., Mirabal, N., Udalski, A., Szymanski, M., Kaluzny, J., Kubiak, M., Krzeminski, M., & Stanek, K. Z. 1996, *ApJ*, 458, L13.
- Mateo, M., Udalski, A., Szymanski, M., Kaluzny, J., Kubiak, M., & Krzeminski, W. 1995, *AJ*, 109, 588
- Moore, B., & Davis, M. 1994, *MNRAS*, 270, 209.
- Oh, K. S., Lin, D. N. C., & Aarseth, S. J. 1995, *ApJ*, 442, 142.

Olszewski, E. W. 1998, in “Galactic Halos: a UC Santa Cruz Workshop,” ASP Conf Series 136, edited by D. Zaritsky (ASP: San Francisco), p. 70.

Piatek, S., & Pryor, C. 1995, AJ, 109, 1071.

Schlegel, D. J., Finkbeiner, D. P., & Davis, M. 1998, ApJ, 500, 525.

Siegel, M. H., Majewski, S. R., Reid, I. N., Thompson, I, Landolt, A. U., & Kunkel, W. E. 1997, BAAS, 29, 1341.

Velazquez H., & White S. D. M. 1995, MNRAS, 275, L23.

Zhao, H-S. 1998, preprint (astro-ph/9804304-v2).

Figure Captions

Figure 1 – A chart showing the locations of the Sgr (open squares) and control fields (open circles). Also noted are the Sgr globular clusters (M 54, Ter 7, Ter 8 and Arp 2), and the foreground cluster M55 (see Mateo et al. 1996; Fahlman et al. 1996). We also plot the approximate extent of Sgr from Ibata et al. (1997; small ellipse denoted ‘IGI’), and where Alard (1996; large rectangle denoted ‘A’) and the Macho team (Alcock et al. 1997; rectangle denoted ‘Macho’) found RR Lyr stars. The large dashed ellipse is the approximate extent of Sgr after these studies and the work of Ibata et al. (1997). The short dashed line corresponds to the SB break seen in Figure 3.

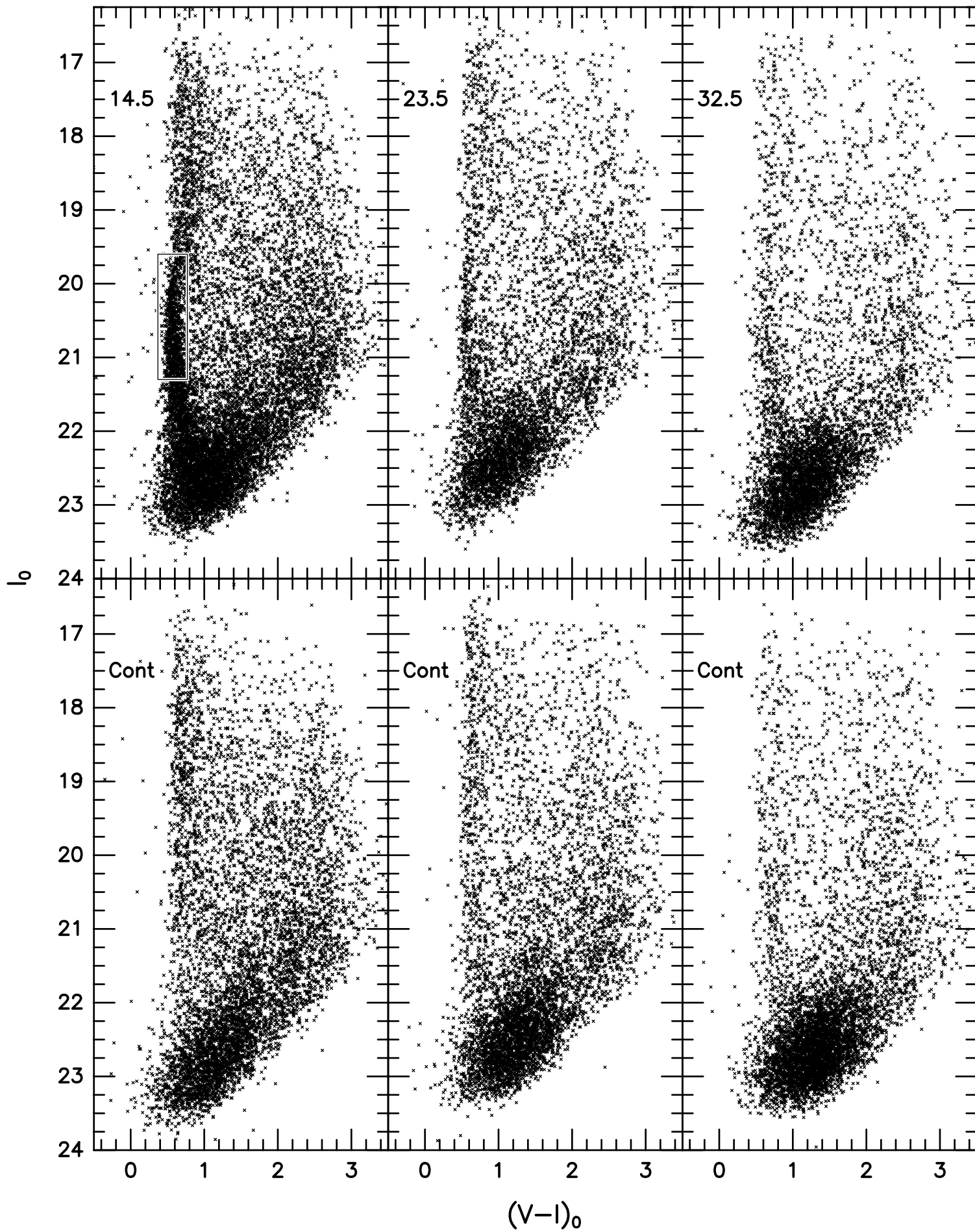
Figure 2 – Dereddened color-magnitude diagrams of Sgr Fields 3, 10 and 16 (upper panels; R is labeled in each panel; see Table 1), and the corresponding three control fields (lower panel). The upper-left panel shows the main-sequence box used to count stars. The extinction parameters were taken from Schlegel et al. (1998).

Figure 3 – *Upper panel:* The raw star counts in the main-sequence box (see Figure 2) as a function of R for both the major-axis Sgr fields (filled squares), and the control fields (filled circles). A linear fit to the control data is shown as a dashed line. The effects of systematically increasing the field reddenings by 0.03 mag (in $(V-I)$) is shown by the upper dash associated with each point, while the lower dashes show the effects of lowering the reddening by 0.03 mag. *Lower panel:* The net counts in each Sgr major-axis field as a function of R (angular distance from M54). The large dashes above and below each data point have the same meaning as in the upper panel. *The conventional error bars denote the Poisson uncertainties of each point.* The dotted line represents the composite exponential profile described in Section 4. The raw and net counts are listed in Table 1.

TABLE 1
LOG OF OBSERVED FIELDS

Field	α_{2000}	δ_{2000}	l deg	b deg	E(V-I) mag	R deg	$N_{MS,raw}$	N_{sky}	$N_{MS,net}$	σ_{net}
1	19 40 22	-33 13 37	6.47	-24.05	0.11	10.0	1458	214.8	1243.2	40.9
2	19 47 23	-33 32 57	6.61	-25.55	0.20	11.5	1382	204.4	1177.6	39.8
3	19 54 27	-33 50 48	6.76	-27.04	0.10	13.0	910	194.4	715.6	33.2
3-N1	19 56 33	-31 53 46	9.00	-26.92	0.18	13.0	932	194.4	737.6	33.6
3-N2	19 58 34	-29 56 36	11.23	-26.76	0.12	13.0	722	194.4	527.6	30.3
3-S1	19 52 15	-35 47 42	4.51	-27.13	0.12	13.0	735	194.4	540.6	30.5
3-S2	19 49 56	-37 44 26	2.27	-27.18	0.12	13.0	348	194.4	153.6	23.3
4	20 01 34	-34 07 08	6.90	-28.54	0.10	14.5	957	185.0	772.0	33.8
5	20 08 43	-34 21 54	7.06	-30.03	0.11	16.0	708	176.0	532.0	29.7
6	20 15 55	-34 35 06	7.21	-31.52	0.10	17.5	559	167.5	391.5	27.0
7	20 23 09	-34 46 43	7.38	-33.02	0.05	19.0	465	159.4	305.6	25.0
8	20 30 25	-34 56 43	7.54	-34.51	0.04	20.5	332	151.6	180.4	22.0
9	20 37 43	-35 05 05	7.72	-36.00	0.04	22.0	308	144.3	163.7	21.3
10	20 45 02	-35 11 48	7.90	-37.50	0.06	23.5	295	137.3	157.7	20.8
11	20 52 22	-35 16 53	8.08	-38.99	0.06	25.0	247	130.6	116.4	19.4
12	20 59 43	-35 20 17	8.28	-40.48	0.07	26.5	268	124.3	143.7	19.8
13	21 07 04	-35 22 01	8.48	-41.97	0.08	28.0	232	118.2	113.8	18.7
14	21 14 26	-35 22 05	8.70	-43.47	0.09	29.5	231	112.5	118.5	18.5
15	21 21 47	-35 20 29	8.92	-44.96	0.11	31.0	169	107.1	61.9	16.6
16	21 29 08	-35 17 12	9.16	-46.45	0.11	32.5	160	101.9	58.1	16.2
17	21 36 28	-35 12 16	9.41	-47.94	0.05	34.0	194	96.9	97.1	17.1
Control fields										
1-Cont	19 23 11	-44 33 53	353.53	-24.05	0.09	...	180	214.8	-34.8	19.9
3-Cont	19 39 18	-45 31 24	353.24	-27.04	0.06	...	222	194.4	27.6	20.4
4-Cont	19 47 33	-45 56 49	353.10	-28.54	0.04	...	172	185.0	-13.0	18.9
7-Cont	20 12 59	-46 59 15	352.62	-33.02	0.04	...	181	159.4	21.6	18.4
10-Cont	20 39 14	-47 39 50	352.10	-37.50	0.04	...	157	137.3	19.7	17.2
13-Cont	21 06 00	-47 57 28	351.52	-41.97	0.04	...	116	118.2	-2.2	15.3
16-Cont	21 32 51	-47 51 38	350.84	-46.45	0.03	...	291	101.9	-10.9	13.9

Mateo et al. -- Figure 2



Mateo et al. -- Figure 3

